JCTC Journal of Chemical Theory and Computation

Transferability of Atomic Properties in Molecular Partitioning: A Comparison

Yu Zhang* and Adam Wasserman

Department of Chemistry, Purdue University, 560 Oval Drive, West Lafayette, Indiana 47907

Received May 10, 2010

Abstract: For a given choice of fragmentation of a molecule, Partition Density Functional Theory (PDFT) provides fragment densities that add up to the correct molecular density, and produce the—in principle exact—molecular energy. Using a simple model system of a heteronuclear diatomic molecule, we investigate the transferability of the resulting PDFT fragment densities by examining how their shapes and dipoles are preserved as the environment changes, and compare with other partitioning schemes. Our results show that (1) the transferability of PDFT densities is about an order of magnitude higher than that of real-space partitioning schemes, and (2) the PDFT *dipoles* are about an order of magnitude more transferable than Hirshfeld dipoles in regions of chemical relevance.

1. Introduction

Partition Density Functional Theory (PDFT), introduced in refs 1, 2 and summarized in the next Section, is a method for calculating molecular properties from Kohn−Sham calculations on isolated fragments. This method was born from the union of the Partition Theory of ref 3 and Kohn−Sham Density Functional Theory.[4] One of the outcomes of a molecular PDFT calculation is a set of fragment densities that can be taken as a convenient alternative to the various definitions of "atoms-in-molecules" (AIMs) proposed over the years by many authors.[5−8] These are useful to define formal charges, local dipoles, and as conceptual tools to understand chemical reactivity.[9,10] In addition, they are also useful *computational* tools. For example, as we explain in the next section, the first step in a PDFT calculation for the ground-state energy of a molecule requires knowledge of a set of densities that add up approximately to the correct molecular density. One could use isolated-atom densities, but the closer the sum of these densities is to the correct molecular density, the faster the convergence of the PDFT equations (at convergence, the resulting fragment densities add up in principle to the *exact* molecular density).

Like other fragment-based computational methods,[11] the appeal of PDFT lies in its promise to allow for electronic-structure calculations that scale linearly with system size.[12] It is thus desirable that the fragment densities be as *transferable* as possible, in the sense that once obtained for a given system, they can be used effectively as the starting point for efficient electronic-structure calculations on other systems.

Our purpose in this work is to study the transferability of PDFT densities. We explore in detail a model system where all quantities can be obtained exactly for different partitioning schemes, compare them with each other, and reveal this way some of the key differences in transferability that are likely to appear in typical applications of AIMs. The model system we study is the same that was recently solved analytically in ref 13. At least in this model of a heteronuclear diatomic molecule, we find that the PDFT densities are significantly more transferable than those arising from other popular schemes. We also show that the PDFT dipoles are in a sense more chemically meaningful than those given by competing methods.

2. Self-Consistent Density Partitioning

An analogy between KS-DFT and PDFT provides a good way to explain the essence of PDFT.[1] Consider the simplest real-life example of interacting electrons, the He atom, and the simplest real-life example of interacting fragments, the H_2^+ molecule. In KS-DFT, the ground-state density of He is expressed as the sum of two densities, i.e., those of the two

* To whom correspondence should be addressed. E-mail: zhang339@purdue.edu.

10.1021/ct100247q
Published on Web 09/29/2010

particles composing the fictitious Kohn−Sham system of *noninteracting electrons*. Similarly, in PDFT, the ground-state density of the H_2^+ molecule is given by the sum of two densities: those of the two fragments composing a fictitious system of *noninteracting fragments*. In KS-DFT, there is a global potential $v_s(\mathbf{r})$ shared by the two noninteracting electrons. In PDFT, there is a global *partition potential* $v_p(\mathbf{r})$ shared by the two noninteracting fragments.

The method works like this: First, we choose a way to fragment the system, that is, assign the nuclei into different fragments. Examples of *binary fragmentation* have been worked out,[2,13] where each atom of a diatomic molecule constitutes in itself a fragment. But a fragment in a molecule could well be a set of atoms characterizing a functional group in organic molecules, or whole amino acids in proteins, or nucleotides in DNA, etc. The number of fragments N_f into which one wishes to partition the molecule plays a role that is analogous to that of the number of electrons N in DFT. Denoting the molecular 1-body potential as $v(\mathbf{r})$, it is decomposed as $v(\mathbf{r}) = \sum_{\alpha=1}^{N_f} v_\alpha(\mathbf{r})$, where $v_\alpha(\mathbf{r})$ is the α^{th} -fragment potential. Fragment α contains N_α electrons, not necessarily an integer (e.g., example of H_2^+ above, where $N_\alpha = 0.5$), but $N = \sum_\alpha^{N_f} N_\alpha$ is obviously an integer. To correctly treat noninteger numbers, we obtain the fragment energy $\mathcal{E}_\alpha$ via the two-component ensemble of Perdew, Parr, Levy, and Balduz[14] (PPLB):

$$\mathcal{E}_\alpha = (1 - \nu_\alpha)E_\alpha[n_{p_\alpha}] + \nu_\alpha E_\alpha[n_{p_\alpha+1}] \tag{1}$$

where p_α is the lower bordering integer of N_α, so: $N_\alpha = p_\alpha + \nu_\alpha$, and $0 < \nu_\alpha < 1$. The energy $E_\alpha[n_{p_\alpha}]$ is that of a system of p_α electrons in the presence of the external potential $v_\alpha(\mathbf{r})$ for fragment α.

The fragment densities $\{n_\alpha(\mathbf{r})\}$ are then obtained by minimizing the total fragment energy $E_f = \sum_\alpha \mathcal{E}_\alpha$ subject to the constraints that $N = \sum_\alpha^{N_f} N_\alpha$, and that $n(\mathbf{r}) = \sum_\alpha n_\alpha(\mathbf{r})$, the total density. Such constrained minimization needs two Lagrange multipliers: the chemical potential μ to guarantee satisfaction of the number constraint, and the *partition potential* $v_p(\mathbf{r})$ to guarantee satisfaction of the *density* constraint. Like the chemical potential, $v_p(\mathbf{r})$ is a global property of the system - the same for all fragments. Like the Kohn−Sham potential, it is a local potential for the electrons within each fragment, and it is "the" potential that yields the set of $\{n_\alpha\}$ adding to the true interacting molecular density. In fact, the fragment density $n_\alpha(\mathbf{r})$ is the ensemble ground-state density for N_α electrons in the external potential $v_\alpha(\mathbf{r}) + v_p(\mathbf{r})$ (for the important proof of uniqueness of $v_p(\mathbf{r})$, see ref 15 where $v_p(\mathbf{r})$ was termed a "reactivity potential").

Since we do not know the total density $n(\mathbf{r})$ in advance, a practical scheme is needed. To that end, the *partition energy* E_p is defined as the difference between the exact energy E and the fragment energy E_f:

$$E_p[\{n_\alpha\}] = E[n] - E_f[\{n_\alpha\}] \tag{2}$$

This is analogous to defining the Hartree-exchange-correlation energy E_{HXC} in KS-DFT as the difference between the exact energy and the sum $T_s[n] + \int d\mathbf{r} v_{ext}(\mathbf{r})n(\mathbf{r})$ (non-interacting kinetic energy plus energy due to external potential). The analogy continues: just like practical KS-DFT calculations rely on approximations to E_{HXC} as a functional of the ground-state density, the success of PDFT will ultimately rely on the quality of approximations of E_p as a functional of the set of fragment densities $\{n_\alpha\}$. The partition potential is given by $\delta E_p[\{n_\alpha\}]/\delta n_\alpha(\mathbf{r})$, for any fragment α. Thus, approximating $E_p[\{n_\alpha\}]$ as a functional of the set of fragment densities leads to a definite prediction for $v_p(\mathbf{r})$, which in turns yields a unique set of $\{n_\alpha(\mathbf{r})\}$, and therefore a prediction for the total molecular density and total fragment energy (from which the true ground state energy $E = E_p + E_f$ is deduced).

In principle, any electronic-structure method could be used in conjunction with the scheme above to solve for the fragment densities and energies. The connection with Kohn−Sham DFT was derived in ref 1. Here, since we deal with a model system[13] whose partition potential and fragment densities can be obtained analytically, numerical self-consistent calculations are not needed. Our goal is to study the transferability of fragments obtained via *exact* PDFT, and compare it with that of other density-partitioning schemes.

In the next Section we define the transferability measures to be used, and in Section 4 we provide a direct comparison between the different methods.

3. Shape Transferability

Rigorous discussions on the mathematical foundation of transferability can be found in ref 16. Here we use an intuitive definition for the transferability of molecular properties. Given a recipe to calculate a molecular property P_M for a molecule M from the set of fragment densities $\{n_\alpha^M(\mathbf{r})\}$, and the set of their centers of gravity $\{\mathbf{r}_\alpha^M\}$, we say that a fragment β common to two different molecules M and M′ is P-transferable from M to M′ if using n_β^M in place of $n_\beta^{M'}$ leads via the same recipe to a value of P that is "close enough" to that of $P_{M'}$. For example, we discuss below the case of μ-transferability, where the recipe to calculate the dipole moment μ is as follows:

$$\boldsymbol{\mu}_M = \sum_\alpha (\boldsymbol{\mu}_\alpha^M - \mathbf{R}_\alpha^M N_\alpha^M) \tag{3}$$

The α^{th}-dipole is measured with respect to an origin placed at $\mathbf{R}_\alpha^M$,

$$\boldsymbol{\mu}_\alpha^M = \int d\mathbf{r}\, n_\alpha^M(\mathbf{r} - \mathbf{R}_\alpha^M)\mathbf{r} \tag{4}$$

For reasons that are made clear in the first paragraph of Section 4.5, we focus here on *shape transferability*, where rather than testing the adequacy of $n_\beta^M(\mathbf{r})$ for predicting properties of M′, we test the adequacy of the shape function[17,18]

$$g_\beta^M(\mathbf{r}) \equiv n_\beta^M(\mathbf{r})/N_\beta^M \tag{5}$$

where N_β^M is the number of electrons of fragment β in molecule M, not necessarily an integer. The degree of μ-transferability of fragment β is thus measured by the smallness of:

$$\Delta\boldsymbol{\mu}^{\beta}_{\mathrm{M}'\to\mathrm{M}} = \int \mathrm{d}\mathbf{r}\, N^{\mathrm{M}}_{\beta}\mathbf{r}[g^{\mathrm{M}'}_{\beta}(\mathbf{r}-\mathbf{R}^{\mathrm{M}}_{\beta}) - g^{\mathrm{M}}_{\beta}(\mathbf{r}-\mathbf{R}^{\mathrm{M}}_{\beta})] \tag{6}$$

We shall also compute

$$D^{\beta}_{\mathrm{M}'\to\mathrm{M}} = \int \mathrm{d}\mathbf{r}\, (N^{\mathrm{M}}_{\beta})^2[g^{\mathrm{M}'}_{\beta}(\mathbf{r}-\mathbf{R}^{\mathrm{M}}_{\beta}) - \mathbf{g}^{\mathrm{M}}_{\beta}(\mathbf{r}-\mathbf{R}^{\mathbf{M}}_{\beta})]^2 \tag{7}$$

which is a measure of the density transferability of fragment β from M′ to M.

4. Comparison

Out of the many existing partitioning schemes, we choose four that do not rely on the use of basis functions. The first two split the density in real space, yielding *nonoverlapping* "atomic" densities (Bader[7] and Voronoi[8]). The last two, by contrast, yield *overlapping* densities (Hirshfeld[6] and PDFT[1]). We apply the four schemes to a simple model system of a heteronuclear diatomic molecule where all quantities can be obtained analytically. Our model consists of two noninteracting electrons moving in one dimension in the presence of two attractive δ-function potentials of strengths $-Z_{\mathrm{A}}$ and $-Z_{\mathrm{B}}$, with $0 < Z_{\mathrm{B}} < Z_{\mathrm{A}}$, a distance $|R_{\mathrm{A}} - R_{\mathrm{B}}| \equiv R$ apart. This model was explored in detail in ref 13, where its relevance for understanding electron localization upon dissociation was discussed. When $Z_{\mathrm{A}} = 1.05$ and $Z_{\mathrm{B}} = 0.95$, the true ionization energy of lithium hydride (0.3 a.u.) is obtained for $R = 2$ a.u. Although the model is admittedly a caricature of the LiH molecule, it nevertheless retains some of the essential elements of real closed-shell heteronuclear diatomic molecules: 2 nuclei with different effective charges (one slightly higher than 1, the other slightly less than 1), 2 active electrons, a permanent dipole moment, density cusps at the nuclei, and exponential decay of the density at large distances, with a decay constant determined by the ionization energy of the most electronegative atom. We therefore expect our comparison to be meaningful for real heteronuclear diatomic molecules.

Since there are two electrons, the total molecular density is given by:

$$n(x) = 2|\psi(x)|^2 \tag{8}$$

where the molecular orbital $\psi(x)$ has the piecewise expression:

$$\psi(x) = \begin{cases} C\mathrm{e}^{\kappa(R/2+x)}, & x < -R/2 \\ D\mathrm{e}^{\kappa x} + F\mathrm{e}^{-\kappa x}, & -R/2 \leqslant x \leqslant R/2 \\ G\mathrm{e}^{\kappa(R/2-x)}, & x > R/2 \end{cases} \tag{9}$$

The wavenumber κ is given by the solutions of the transcendental equation:

$$(\kappa - Z_{\mathrm{A}})(\kappa - Z_{\mathrm{B}}) = \mathrm{e}^{-2\kappa R} Z_{\mathrm{A}} Z_{\mathrm{B}} \tag{10}$$

and the constants C, D, F, and G are given explicitly in the Appendix in terms of κ, Z_{A}, Z_{B}, and R.

We now propose one-dimensional versions that capture the main features of the four partitioning schemes, and apply them to our model system:

4.1. Bader. Bader's Atoms-in-Molecules scheme[7] uses zero-flux surfaces to partition the entire space. These are defined as the surfaces through which the divergence of the electron density $\nabla n(\mathbf{r})$ has no flux. In one-dimensional systems, the dividing "surfaces" collapse to points where $dn(x)/dx = 0$. Bader's A-fragment density in our model system is thus identical to $n(x)$ for all x less than $x_{\mathrm{Bader}} \equiv (1/2\kappa)\ln(F/D)$, and zero otherwise:

$$n^{\mathrm{Bader}}_{\mathrm{A}}(x) = \begin{cases} n(x), & x < (1/2\kappa)\ln(F/D) \\ 0, & \text{otherwise} \end{cases} \tag{11}$$

The left panel of Figure 1 compares this fragment density (solid line) with an isolated atom density when the choice of parameters is such that $n(x)$ is almost symmetric, having $F \approx D$ and therefore $x_{\mathrm{Bader}} \approx 0$.

4.2. Voronoi. In this scheme, the atomic basins are bounded by planes perpendicular to the interatomic bonds. According to the original proposal of Voronoi,[19] the dividing planes should be located at the midpoints of the interatomic bonds, but a modified version[8] puts them at a distance $R_{\mathrm{A}} = (X_{\mathrm{A}}/(X_{\mathrm{A}} + X_{\mathrm{B}}))R$ from nucleus A, where R is the distance between nuclei A and B, and the $X_{\mathrm{A,B}}$'s are the van der Waals radii of atoms A and B. In our one-dimensional model, since the nuclear radii are ill-defined, we locate the dividing "planes" at distances $R_{\mathrm{A}} = (Z_{\mathrm{B}}/(Z_{\mathrm{A}} + Z_{\mathrm{B}}))R$ instead, where Z_{A} and Z_{B} are the nuclear charges. Voronoi's A-fragment density is then identical to $n(x)$ for all x less than $x_{\mathrm{Voronoi}} \equiv R[Z_{\mathrm{B}}/(Z_{\mathrm{A}} + Z_{\mathrm{B}}) - 1/2]$:

$$n^{\mathrm{Voronoi}}_{\mathrm{A}}(x) = \begin{cases} n(x), & x < R\left[Z_{\mathrm{B}}/(Z_{\mathrm{A}} + Z_{\mathrm{B}}) - \frac{1}{2}\right] \\ 0, & \text{otherwise} \end{cases} \tag{12}$$

The second panel of Figure 1 shows this density for a choice of parameters such that $Z_{\mathrm{B}}/(Z_{\mathrm{A}} + Z_{\mathrm{B}}) \approx 1/2$, and therefore $x_{\mathrm{Voronoi}} \approx x_{\mathrm{Bader}}$.

4.3. Hirshfeld. The one-dimensional version does not require any modification of Hirshfeld's original proposal.[6] Here, the α^{th}-fragment density $n_{\alpha}(x)$ is found by multiplying the molecular density $n(x)$ by a weight function $w_{\alpha}(x)$ given by the ratio $n^0_{\alpha}(x)/n^0(x)$, where $n^0_{\alpha}(x)$ is the density of fragment α when truly isolated, and $n^0(x) = \sum_{\alpha} n^0_{\alpha}(x)$. For our model system, the truly isolated A-atom density is the simple exponential $n^0_{\mathrm{A}}(x) = Z_{\mathrm{A}} e^{-2Z_{\mathrm{A}}|x+R/2|}$, so

$$n^{\mathrm{Hirshfeld}}_{\mathrm{A}}(x) = n(x)\left[1 + \frac{Z_{\mathrm{B}}}{Z_{\mathrm{A}}}\left(\frac{\exp\left(-2Z_{\mathrm{A}}\left|x + \frac{R}{2}\right|\right)}{\exp\left(-2Z_{\mathrm{B}}\left|x - \frac{R}{2}\right|\right)}\right)\right]^{-1} \tag{13}$$

The third panel in Figure 1 shows how $n^{\mathrm{Hirshfeld}}_{\mathrm{A}}$ extends over all space (solid line), and resembles $n^0_A(x)$ (dotted line).

4.4. PDFT. We applied the method as described in Section 2. The A-fragment density was found analytically in ref 13. It is conveniently expressed as follows:

$$n^{\mathrm{PDFT}}_{\mathrm{A}}(x) = n(x)(1 + \sin 2\beta(x))/2 \tag{14}$$

where $\beta(x)$ is an auxiliary polar-angle function given by:

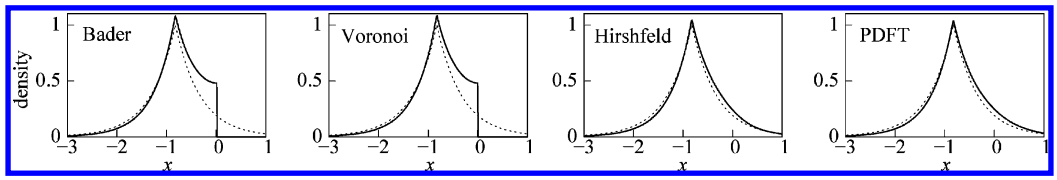

Figure 1. Comparison of A-fragment densities for four different density-partitioning schemes applied to the 1dAB model with $\Delta Z = 10^{-2}$, $\bar{Z} = 1$, and $R = 1.65$. The dotted lines show the isolated-atom density: $Z_A e^{-2Z_A|x+R/2|}$.

$$\beta(x) = \begin{cases} \beta_A, & x < -\dfrac{R}{2} \\ \beta_A + \alpha_1\left(\alpha_2 - \dfrac{e^{-2\kappa x}}{De^{(2\kappa x)} + F}\right), & -\dfrac{R}{2} \leqslant x \leqslant \dfrac{R}{2} \\ \beta_B, & x > -\dfrac{R}{2} \end{cases} \tag{15}$$

The values for the constants β_A, β_B, α_1, and α_2 are provided in the Appendix.

The right panel in Figure 1 shows $n_A^{PDFT}(x)$ when $Z_A = 1.005$, $Z_B = 0.995$, and $R = 1.65$. The distortion of the PDFT fragment density with respect to the isolated-atom density equals that of Hirshfeld's to first-order in $\Delta Z \equiv Z_A - Z_B$. However, to higher orders of ΔZ, the differences will prove important, as we discuss next.

4.5. "Atomic" Densities and Dipoles. It is clear from Figure 1 that Bader and Voronoi densities belong to a different family than those of Hirshfeld and PDFT. The overlapping densities (Hirshfeld and PDFT) resemble atomic densities, but differ from them in a meaningful way. It might seem at first sight from Figure 1 that the Hirshfeld and PDFT schemes yield identical densities, but careful examination shows that the PDFT density of the most electronegative atom (A in this case) exhibits a slower decay in the bonding region (range $0 < x < 1$ in Figure 1). Interestingly, since all atomic dipoles vanish as $R \to \infty$, these subtle differences are large enough to determine the *sign* of the dipole at large but finite R.

Figure 2 shows the electronic dipole moment for the A-fragment (1d-version of eq 4) as a function of inter-"nuclear" separation R. Chemically, it makes sense to expect the sign of μ_A to be positive for all R. Indeed, as the negative charge density on the A-atom is pulled by the unscreened positive charge on the B-atom, the fragment density for the A-atom becomes asymmetric. There is more negative charge on the right-hand side of the A-nucleus than on the left. So, a chemically reasonable fragment density for the A-atom should be expected to exhibit a positive dipole at all internuclear separations. PDFT is the only scheme that satisfies this (see upper panel in Figure 2). The slower decay of $n^{PDFT}(x)$ compared to $n^{Hirshfeld}(x)$ in the bonding region, hardly visible in Figure 1 (the effect is second order on ΔZ), is in fact crucial to determine the "correct" sign of the dipole moment at large R, where Hirshfeld's becomes negative. We use quotes for *correct* because the fragment dipole is of course not measurable at finite R. The Bader and Hirshfeld dipoles switch sign at $R \approx 1.4$ and 2.2 respectively, and the Voronoi dipole is always negative. The lower panels in Figure 2 show the actual A-fragment densities at small and large R, explaining the observed sign of μ_A.

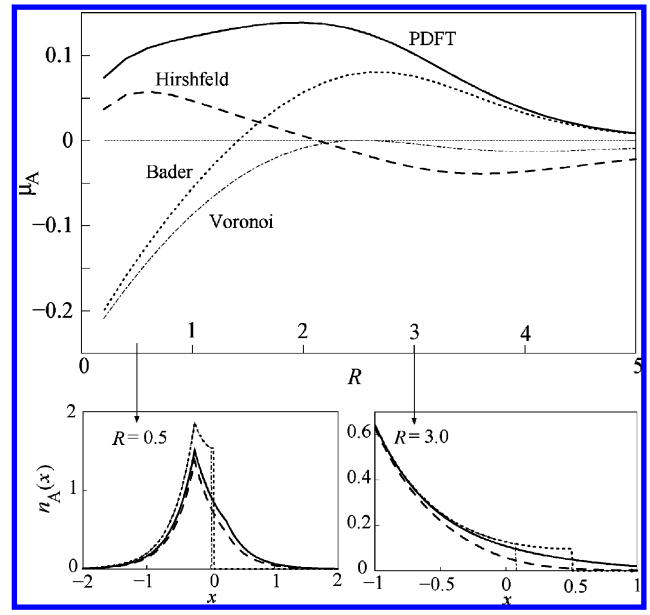

Figure 2. Top panel: Fragment dipole eq 4 for the A-atom as a function of inter"nuclear" separation when $Z_A = 1.05$, and $Z_B = 0.95$. Bottom panels: Density of A-atom from the four different schemes when $R = 0.5$ (*left*) and $R = 3.0$ (*right*).

We make two more points based on Figure 2: (1) The densities from overlapping schemes preserve their atomic-like shapes even for very small Rs. This is achieved partly because at small internuclear separations, the B-atom contributes significantly to the molecular density at the position of the A-nucleus; (2) For large values of R, because of its slower decay in the bonding region, the PDFT density for the A-atom runs closer than Hirshfeld's to the exact molecular density.

4.6. *n*-Transferability. When ΔZ is changed for fixed R, the fragment densities change in a way that can be understood by examining two separate effects: change of *shape*, and change of *number*. As $R \to \infty$, only the *number* effect is important (for A) because $n(x)$ becomes equal to the sum of two purely atomic densities containing noninteger numbers of electrons. At truly infinite separation, the 2 electrons sit close to the most electronegative atom (A), and the density becomes equal to twice the density of the 1-electron A-atom (since electrons are not interacting in our model). At small R, however, charge transfer is less important. For example, when ΔZ is changed from 0 to 10^{-4} the B-atom retains more than 99% of its single electron for all separtions lower than $R = 5$. The main effect then is a change of *shape*. It is thus convenient to separate the two effects, as indicated in Section 3, eqs 6 and 7.

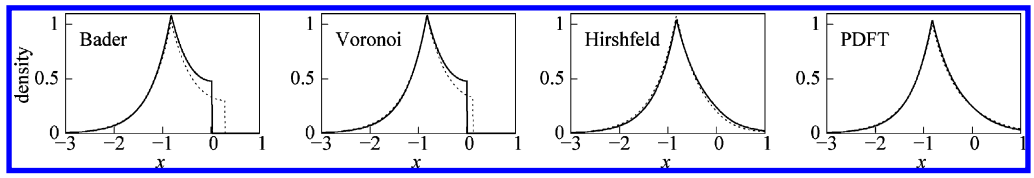

Figure 3. Fragment densities for the A-atom when $Z_A = 1.005$ and: *solid lines*: $Z_B = 0.995$, and $R = 1.65$; *dotted lines*: $Z_B = 0.895$, and $R = 1.80$. These have been shifted and renormalized to test shape transferability (see text).

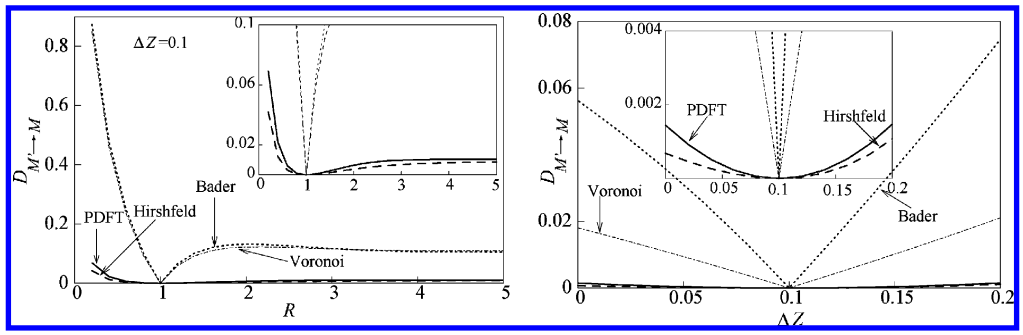

Figure 4. Density transferability as measured by $D_{M'\to M} = \sum_\alpha D^\alpha_{M'\to M}$, eq 7, for the four schemes, when: *Left*: the reference molecule M′ corresponds to $R = 1$, with $\Delta Z = 0.1$, and the tested molecules M have the same value of ΔZ but different R's; *Right*: the reference molecule has $R = 1$ and $\Delta Z = 1$, and the tested molecules M have the same value of R but different ΔZ's.

To that end, we first take the same densities of Figure 1, extract their shapes (eq 5), and multiply them by the number of electrons that the A-atom would have had in a molecule defined by the same value of Z_A but different Z_B and R (this number obviously changes from scheme to scheme). Figure 3 compares the renormalized and shifted A-density of M′ (the new 'molecule') with that of M (the original "molecule"). Clearly, for the set of parameters chosen in Figure 3, the PDFT and Hirshfeld densities are more transferable than those obtained by nonoverlapping schemes. We confirm this is true for *any* choice of parameters by plotting D (defined in eq 7) for fixed ΔZ as a function of R (left panel of Figure 4) and for fixed R as a function of ΔZ (right panel of Figure 4). Similar behavior was observed for all choices of R and ΔZ. We note that the slopes dD/dR and $dD/d\Delta Z$ around the reference point that defines the molecule M ($R = 1$ in the left panel of Figure 4) are more than an order of magnitude smaller for the overlapping than for the nonoverlapping schemes (better seen in the insets), proving the much higher transferability of Hirshfeld and PDFT densities over those based on real-space cutoff procedures. Interestingly, the PDFT scheme is superior to Hirshfeld's in terms of *dipole* transferability, as we show below.

4.7. μ-Transferability. We now fix $Z_A = 1.05$, $Z_B = 0.95$, and $R = 2.0$, a chemically reasonable bond length for this model. The exact molecular dipole is -0.71073 a.u. Table 1 shows the values obtained under the 4 different schemes when Z_B is lowered to 0.9 (keeping Z_A fixed), and the shape of the new fragments is employed to estimate the dipole of the original molecule. The difference with the exact dipole is given by the 1-dimensional version of eq 6 (column 2 in Table 1). Clearly, for $R = 2$, the PDFT densities are the most μ-transferable. Lastly, Figure 5 plots $\Delta\mu_{M'\to M} = \sum_\alpha \Delta\mu^\alpha_{M'\to M}$ as a function of R. PDFT averages over the two nonoverlapping schemes, and does better than Hirshfeld's for all separations larger than ~1. In fact, in this window of internuclear separations, both nonoverlapping schemes show better dipole-transferability than Hirshfeld's. This can be understood in the following way. When decreasing Z_B for fixed Z_A, the change of the molecular density close to nucleus A is a change of *number* of electrons more than shape. This is exactly true when $R \to \infty$, and approximately so for finite R. The change of the molecular density close to B, however, is both of number *and* shape, since the decay of the density is governed by Z_A far from both nuclei. Not having the flexibility to reverse this change of shape upon resizing is the main source of error of nonoverlapping schemes. The error has a negative sign at large distances, indicating that

Table 1. Error for Molecular Dipole when $R = 2$ from the Four Partitioning Schemes[a]

	μ_M	$\Delta\mu_{M'\to M}$	error (%)
Bader	−0.68315	0.02758	3.8
Voronoi	−0.73175	−0.02103	−2.9
Hirshfeld	−0.81283	−0.10210	−14.4
PDFT	−0.70912	0.00161	0.2

[a] Z_A is fixed to 1.05 and Z_B lowered from 0.95 to 0.90 (see text).

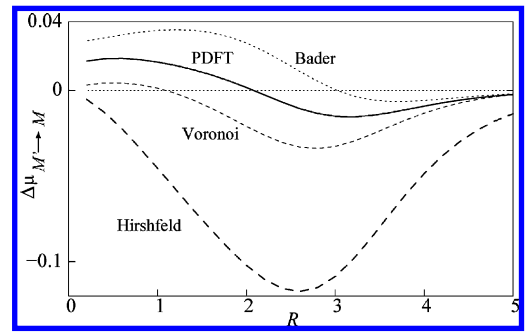

Figure 5. Transferability of the dipole moment as measured by $\Delta\mu_{M'\to M} = \sum_\alpha \Delta\mu^\alpha_{M'\to M}$, eq 6. Here, $Z_A = 1.05$ and Z_B changes from 0.95 for M to 0.90 for M′.

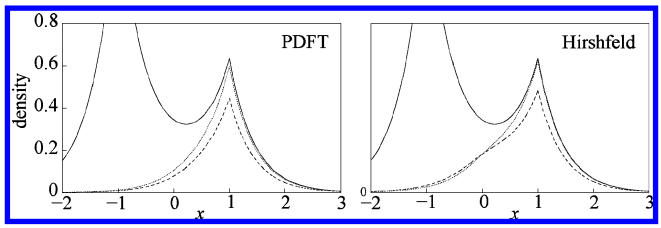

Figure 6. Comparison of the B-densities obtained by PDFT (left) and Hirshfeld (right) when $R = 2$, $Z_A = 1.05$ and Z_B is lowered from 0.95 (thin) to 0.90 (dashed). The solid line shows the full molecular density corresponding to the higher value of Z_B.

too much density leans toward the more electronegative nucleus A, understandably. Why is Hirshfeld's error so much larger? When multiplied by the actual molecular density corresponding to the lower value of Z_B, the isolated-atom density used as a weighting function in Hirshfeld's scheme shifts too much density toward A (right panel in Figure 6). After resizing (i.e., multiplying by a number larger than 1 to get the correct occupation of fragment B for the higher value of Z_B, while keeping the shape of the lower value), this leads to a molecular dipole that is much too negative, effectively squaring the error as compared to nonoverlapping schemes.

5. Conclusions

The results obtained for a simple model of a heteronuclear diatomic molecule highlight some of the advantages of the recently proposed Partition Density Functional Theory[1−3] over other density-partitioning schemes. First, the PDFT fragment-densities are more transferable than those of nonoverlapping schemes such as Bader's and Voronoi's. Second, the resulting PDFT dipoles are better adjusted to chemical intuition, at least in our model system.

We emphasize that PDFT is *not* simply a method to partition the density of a molecule. In fact, *all* molecular properties are encoded into each fragment density, and can be decoded from any of them. When connected to KS-DFT, refs 1 and 2 show how to extract the exact molecular ground-state energy via self-consistent calculations on the PDFT fragments. There is no obvious *a priori* reason to expect the PDFT fragment densities to be more transferable than those obtained by other density-partitioning methods. But the results reported here indicate that the *shapes* of the PDFT fragments are special. They are more transferable than the shapes obtained via other popular methods, either overlapping or nonoverlapping. It will be very interesting to see if the same conclusion holds for real molecules, so we are working on this. If the answer is positive (and we do not see why the picture should change qualitatively for real diatomics), then PDFT fragment densities have a bright future. On the one hand, they will be preferred as starting densities for improving convergence of fragment-based computational methods.[11] On the other hand, they will find good use in many branches of computational chemistry, from QM/MM applications to novel linear-scaling algorithms.

One of the slow steps of PDFT calculations as currently implemented is the simultaneous calculation of the occupation numbers $\{\nu_\alpha\}$ that minimize the partition energy, eq 2. These are of course an important output of a PDFT calculation. But when the main interest is not to compute formal charges, but to calculate molecular energies efficiently, an interesting possibility suggested here is that the approximate shape of the PDFT fragment densities can be found first for a fixed set of $\{\nu_\alpha\}$ (e.g., by imposing integer occupations), and then, simpler population analysis methods can provide occupation numbers to be used in conjuction with PDFT to yield approximate molecular energies.

Acknowledgment. Acknowledgment is made to the Donors of the American Chemical Society Petroleum Research Fund for support of this research under Grant No. 49599-DNI6. Y.Z. would like to thank Jing Zhu and Qi Wei for discussions on *Mathematica* programming.

Appendix

All calculations were accomplished with the *Mathematica* program.[20] To guarantee high precisions, analytical expressions or symbolic operations were involved when available.

The model system constists of two non-interacting electrons under the potential

$$v(x) = -Z_A\delta(x + R/2) - Z_B\delta(x - R/2) \tag{16}$$

where $Z_A > Z_B > 0$. The analytical solution of the 1-d Schrödinger equation with the potential above is shown in eq 9, where

$$\begin{aligned} D &= e^{\kappa R/2}(1 - Z_A/\kappa)C \\ F &= e^{-\kappa R/2}(Z_A/\kappa)C \\ G &= e^{\kappa R}\left(\frac{\kappa - Z_A}{Z_B}\right)C \\ C &= \sqrt{2\kappa}\left\{\frac{Z_A(\kappa - Z_A)}{Z_B(\kappa - Z_B)}\left(1 + \frac{Z_B^2}{\kappa^2}\right) - \frac{e^{-2\kappa R}Z_A^2}{\kappa^2} + \right. \\ &\quad \left. \frac{2Z_A}{\kappa}[1 + 2R(\kappa - Z_A)]\right\}^{-1/2} \end{aligned} \tag{17}$$

For convienence, an auxiliary polar-angle function $\beta(x)$ is introduced.[13] In eq 15, β_A is the solution of the trigonometric equation

$$K_1\cos(2\beta_A) - K_2\cos[2(\beta_A + K_1K_3\cos(2\beta_A)] = 0 \tag{18}$$

and

$$\beta_B = \beta_A + K_1K_3\cos(2\beta_A) \tag{19}$$

where

$$\begin{aligned} K_1 &= -Z_AC^2 \\ K_2 &= -Z_BG^2 \\ K_3 &= \frac{1}{2\kappa D}\left(\frac{e^{\kappa R/2}}{C} - \frac{e^{-\kappa R/2}}{G}\right) \end{aligned} \tag{20}$$

and

$$\alpha_1 = K_1 \frac{\cos(2\beta_A)}{2\kappa D}$$
$$\alpha_2 = \frac{e^{\kappa R/2}}{C} \tag{21}$$

So the charge on atom B is

$$\nu = 1 - \int_{-\infty}^{\infty} |\psi(x)|^2 \sin[2\beta(x)]\, dx \tag{22}$$

where $\psi(x)$ is defined in eq 9. For all the details of the derivation of the equations above, and for explicit expressions for the partition potential $v_p(x)$, please see the Appendix of ref 13.

References

(1) Elliott, P.; Burke, K.; Cohen, M. H.; Wasserman, A. *Phys. Rev. A* **2010**, *82*, 024501.

(2) Elliott, P.; Cohen, M. H.; Wasserman, A.; Burke, K. *J. Chem. Theory Comput.* **2009**, *5*, 827–833.

(3) Cohen, M. H.; Wasserman, A. *J. Phys. Chem. A* **2007**, *111*, 2229–2242.

(4) Kohn, W.; Sham, L. J. *Phys. Rev.* **1965**, *140*, A1133−A1138.

(5) (a) Löwdin, P.-O. *J. Chem. Phys.* **1953**, *21*, 374–375. (b) Mulliken, R. S. *J. Chem. Phys.* **1955**, *23*, 1833–1840. (c) Politzer, P.; Harris, R. R. *J. Am. Chem. Soc.* **1970**, *92*, 6451–6454. (d) Reed, A. E.; Weinhold, F. *J. Chem. Phys.* **1983**, *78*, 4066–4073. (e) Reed, A. E.; Weinstock, R. B.; Weinhold, F. *J. Chem. Phys.* **1985**, *83*, 735–746.

(6) Hirshfeld, F. L. *Theor. Chim. Acta* **1977**, *44*, 129–138.

(7) Bader, R. F. W. *Atoms in Molecules: A Quantum Theory*; Oxford University Press: New York, 1990.

(8) Rousseau, B.; Peeters, A.; van Alsenoy, C. *J. Mol. Struct.: THEOCHEM* **2001**, *538*, 235–238.

(9) Geerlings, P.; De Proft, F.; Langenaeker, W. *Chem. Rev.* **2003**, *103*, 1793–1874.

(10) Parr, R. G.; Yang, W. *Density-Functional Theory of Atoms and Molecules; International Series of Monographs on Chemistry*; Oxford University Press, New York, 1989; pp 221−224.

(11) (a) Wesolowski, T. A.; Warshel, A. *J. Phys. Chem.* **1993**, *97*, 8050–8053. (b) Gadre, S. R.; Shirsat, R. N.; Limaye, A. C. *J. Phys. Chem.* **1994**, *98*, 9165–9169. (c) Kitaura, K.; Ikeo, E.; Asada, T.; Nakano, T.; Uebayasi, M. *Chem. Phys. Lett.* **1999**, *313*, 701–706. (d) Exner, T. E.; Mezey, P. G. *J. Phys. Chem. A* **2002**, *106*, 11791–11800. (e) Zhang, D. W.; Xiang, Y.; Zhang, J. Z. H. *J. Phys. Chem. B* **2003**, *107*, 12039–12041. (f) Li, S. H.; Li, W.; Fang, T. *J. Am. Chem. Soc.* **2005**, *127*, 7215–7226. (g) Huang, L. L.; Massa, L.; Karle, J. *Int. J. Quantum Chem.* **2005**, *103*, 808–817. (h) Deev, V.; Collins, M. A. *J. Chem. Phys.* **2005**, *122*, 154102. (i) Bettens, R. P. A.; Lee, A. M. *J. Phys. Chem. A* **2006**, *110*, 8777–8785. (j) Řezáč, J.; Salahub, D. R. *J. Chem. Theory Comput.* **2010**, *6*, 91–99.

(12) Goedecker, S. *Rev. Mod. Phys.* **1999**, *71*, 1085–1123.

(13) Cohen, M. H.; Wasserman, A.; Car, R.; Burke, K. *J. Phys. Chem. A* **2009**, *113*, 2183–2192.

(14) Perdew, J. P.; Parr, R. G.; Levy, M.; Balduz, J. L. *Phys. Rev. Lett.* **1982**, *49*, 1691–1694.

(15) Cohen, M. H.; Wasserman, A. *J. Stat. Phys.* **2006**, *125*, 1125–1139.

(16) Ayers, P. W. *J. Chem. Phys.* **2000**, *113*, 10886–10898.

(17) Parr, R. G.; Bartolotti, L. J. *J. Phys. Chem.* **1983**, *87*, 2810–2815.

(18) Ayers, P. W. *Proc. Natl. Acad. Sci. U.S.A.* **2000**, *97*, 1959–1964.

(19) Voronoi, G. *J. Reine Angew. Math.* **1907**, *133*, 97–178.

(20) Wolfram Research, Inc., *Mathematica*, Version 6.0, Champaign, IL (2007).

CT100247Q